Electrocatalysis (2015) 6:534–543
DOI 10.1007/s12678-015-0272-z

ORIGINAL RESEARCH

Electrochemical Hydrogen Oxidation on Pt(100): a Combined Direct Molecular Dynamics/Density Functional Theory Study

Juan A. Santana [1,3] · **José J. Saavedra-Arias** [1,2] · **Yasuyuki Ishikawa** [1]

Published online: 9 August 2015

Abstract We have studied the hydrogen oxidation reaction on various catalytic sites at the water/Pt(100) interface with first-principles direct molecular dynamics and minimum energy pathway calculations. The calculations indicate that the mechanism for electro-oxidation of H_2 on terrace sites of the Pt(100) surface depends on the concentration of inactive adsorbed hydrogen on the electrode surface. Near the reversible potential, the electro-oxidation follows the Tafel-Volmer homolytic cleavage of H_2 at low coverage of adsorbed hydrogen. If the surface is covered with ca. 1 monolayer of hydrogen, however, the oxidation proceeds by the Heyrovsky-Volmer mechanism. We found good agreement between measured and predicted Tafel plots, indicating that hydrogen oxidation/reduction reaction on Pt(100) takes place via the Heyrovsky-Volmer mechanism under ca. 1 monolayer coverage of inactive adsorbed hydrogen.

Keywords Electrocatalysis · Surface catalysis · Fuel cells · Proton-coupled electron-transfer · Heyrovsky- and Tafel-Volmer mechanisms

✉ Juan A. Santana
juan.santana6@upr.edu

[1] Department of Chemistry, University of Puerto Rico at Rio Piedras, P.O. Box 23346, San Juan, PR 00931, USA

[2] Department of Physics, Universidad Nacional, Heredia 40101, Costa Rica

[3] Present address: Department of Chemistry, University of Puerto Rico at Cayey, P. O. Box 372230, Cayey, PR 00737-2230, USA

Introduction

The hydrogen evolution reaction (HER) and hydrogen oxidation reaction (HOR) on Pt electrodes are among the most studied electrochemical processes because of their practical importance [1]. The mechanistic details of the electrocatalytic HOR on low-index Pt(*hkl*) single crystals in acid solution has received renewed interest in the recent years because of the potential of hydrogen-based fuel cells [2], where the HOR occurs, for instance, at the anode of the proton-exchange membrane fuel cells.

It is generally accepted that HOR on low-index Pt(*hkl*) single crystals involve the following elementary steps: [3]

$$H_2 \rightarrow H_{ads} + H_{ads} \quad (\text{Tafel}),$$

$$H_2 \rightarrow H_{ads} + H^+ + e^- \quad (\text{Heyrovsky}),$$

$$H_{ads} \rightarrow H^+ + e^- \quad (\text{Volmer}).$$

The overall HOR, $H_2 \rightarrow 2H^+ + 2e^-$, involves H_2 dissociation either by the Tafel or the Heyrovsky reaction step, followed by the oxidation of H_{ads} via the Volmer process.

Despite these apparently simple mechanisms proposed for the HER/HOR on low-index Pt(*hkl*) single crystals, there have been controversies in the literature concerning the detailed reaction mechanism, the nature of the hydrogen intermediate involved, and the effect of the microstructure of the Pt surface on the electrochemical reactions. In early studies, the inability to accurately identify the structure of adsorbates led to the proposal of numerous mechanistic pathways for the electrocatalytic HOR/HER [1]. Several studies reported that the electrochemical HOR/HER was insensitive to the Pt(*hkl*) structure; see Ref. [4] and references therein. Later works, however, found that the kinetics of the HER/HOR on Pt(*hkl*) in alkaline [5] and acid [6] solutions vary with crystal faces. In

acid electrolytes, for instance, a study [6] of the hydrogen electrochemistry found that each crystal face possesses a unique temperature-dependent Tafel slope for the HOR and the activation energies (E_a) for the HER/HOR decreases in the sequence (111)>(100)>(110). These differences in E_a with the crystal faces were attributed to structure-sensitive heats of adsorption of the active intermediate H_{ads} [6], whose physical state is still unclear.

Surface spectroscopic techniques have provided the most atomic scale detailed look at electrocatalytic reactions on Pt polycrystalline [3, 7–10] and low-index single crystal surfaces [3, 7, 11, 12]. In in situ IR spectroscopy studies [3], a Pt-H stretching vibration at 2090 cm^{-1} was identified on Pt polycrystalline and (111) single crystal electrodes at potentials below 110 mV vs. the reversible hydrogen electrode (RHE). The electrochemical hydrogen adsorption on Pt(100), Pt(1111), Pt(110), and Pt(111) electrode surfaces was later studied [11] using in situ IR reflection absorption spectroscopy, and it was shown that the terminal hydrogen adsorption is sensitive to the surface crystallographic orientation. The IR bands of the adsorbed hydrogen on Pt(100), Pt(1111), and Pt(110) were observed at 1990–2080 cm^{-1} at potentials more negative than +0.25 V vs. RHE. A further study [7] with the infrared-visible sum frequency generation (SFG) technique showed the vibrational signature of terminal hydrogen on low-index Pt(*hkl*) at 1800–2020 cm^{-1}. In a more recent work [12], hydrogen adsorption on Pt(*hkl*), and Pt(211), and Pt(311) was studied using in situ IR reflection absorption spectroscopy. In that work [12], the band around 2080 cm^{-1} was observed only for hydrogen adsorbed on Pt(110) and stepped Pt surfaces at potentials near 0 V vs. RHE.

Computational modeling, particularly those based on density functional theory (DFT), have been increasingly employed to study electrochemical reactions [13–15] with different schemes and approximations [16–27] to simulate electrochemical conditions. The mechanistic pathways of the HER/HOR on Pt electrodes have been explored with DFT and model systems of a Pt atom with a solvated H^+ [16], micro-solvated Pt clusters [21], and slab models of the electrolyte/Pt interface [22–26].

In previous studies [21, 28], we conducted first-principles direct molecular dynamics (MD) study of the HOR at the water/Pt(111) interface. Our calculations showed that the HOR on this surface proceeds via the Heyrovsky-Volmer mechanism with H^+ and inert adsorbed bridging hydrogen (H_b) as reaction products. H_b on Pt(111) was identified as the underpotential-deposited hydrogen, the so-called UPD H [21, 28]. On the other hand, a following study [29] revealed that the HOR on the Pt(110) follows the Tafel-Volmer mechanism with hydrogen adsorbed at the on-top site (H_o) as the intermediate species. The Pt-H stretching frequency 2083 cm^{-1} was predicted for H_o on Pt(110) near the reversible potential, in agreement with the IR band at 2080 cm^{-1} [11, 12].

In the present study, the mechanistic details of the HOR on Pt(100) are examined in detail using direct MD simulation and DFT methods. We address the adsorbed UPD states of hydrogen and their possible involvement in the electrocatalytic processes. The mechanisms for the formation of UPD H on Pt(100) at ca. 1 monolayer (ML) coverage are still not well understood, and thus, a detailed theoretical study is expected to complement previous experimental [6] and theoretical studies [16, 26]. E_a for the oxidation of hydrogen on Pt(100) is calculated and compared with those on Pt(110) and Pt(111), and experiment. The study will help to approach an understanding of the relationship between the electrocatalytic behavior of the anodic HOR and the adsorbed UPD state of hydrogen at low- and high-coverage states at the water/Pt(100) interface.

Computational Details

To study the electrochemical hydrogen oxidation at the water/Pt(100) interface, we employed a cluster model. The oxidation mechanism was established performing direct MD based on DFT. The direct MD results were then verified with minimum energy pathway (MEP) calculations. In this section, we describe the DFT calculations, cluster models, electrode potential modeling, and the MEP and direct MD calculations.

DFT calculations were carried out with the DMol [3] software package [30]. We used double numerical quality basis sets with polarization functions (DNP) [30] to expand the Kohn-Sham orbitals and the Perdew-Burke-Ernzerhof (PBE) [31] exchange-correlation functional. DNP basis sets minimize superposition errors and correctly describe molecular polarizabilities [30]. For geometry relaxation, the core potentials were represented with DFT semi-local pseudo-potentials (DSPP). Final total energies were then evaluated with an all-electron scalar relativistic algorithm [30] to obtain accurate energies. The combination of PBE and the all-electron scalar relativistic algorithm implemented in Dmol [3] has been shown to be accurate for binding and reaction energy of hydrogen on Pt surfaces [21, 29]. The technique [30] of fractional occupation numbers was used applying a Fermi smearing of 0.1 eV to accelerate the convergence of the Self-Consistent-Field (SCF) procedure.

Metal clusters with 37 and 39 Pt atoms (Fig. 1) were used to simulate Pt(100) with terrace and (111) step sites, respectively. Cluster thickness effects on the energetics of hydrogen on Pt(100) are expected to be below 1 kcal/mol [21, 29]. The binding energy of H_o on clean Pt(100) and at water/Pt(100) interface calculated with our models are 64 and 63 kcal/mol, respectively. For H_b on clean Pt(100) and at water/Pt(100) interface, calculations with our models yield 67 and 68 kcal/mol, respectively. These results are in good agreement with the measured values for hydrogen on Pt(100) under high

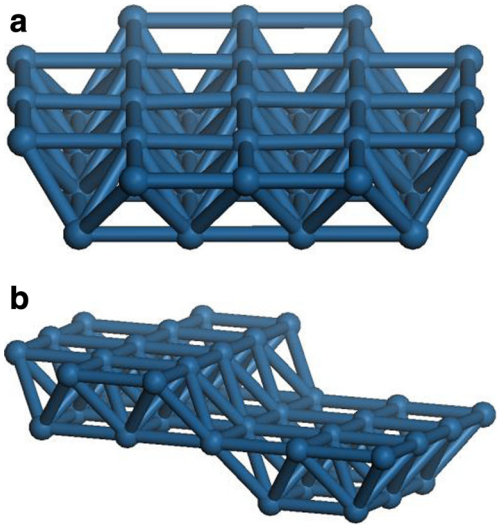

Fig. 1 Cluster models employed to simulate **a** $Pt_{37}(100)$ terrace sites and **b** $Pt_{39}(100)$ with (111) step sites

vacuum [32] and electrochemical conditions [33, 34], i.e., 63 and 64–65 kcal/mol, respectively. A similar agreement was found for hydrogen Pt(111), where our calculations with the two-layer cluster model yielded [21] a hydrogen binding energy of 56 kcal/mol, in close agreement with the experimental value [35] 57–60 kcal/mol. Moreover, the binding energy of hydrogen on Pt(111) evaluated with our cluster models agrees with calculations from extended surface models [21].

The water/Pt(100) interface was created by adding up to 18 water molecules on one side of the cluster models. Geometry optimizations of the water/Pt(100) systems were performed by allowing all solvent water molecules and the top layer of the Pt clusters to relax freely until residual forces were below 0.03 eV/Å. The bottom layer of the Pt clusters was held fixed to the experimental position of bulk Pt, a=3.92 Å.

As in our previous works [21, 29], the effective electrode potential in the Pt clusters was controlled adding/removing a given number of electrons (charge q) to/from the water/Pt(100) systems. In our method, the electrode potential $U(q)$ is established by a linear interpolation of two characteristic potentials: (i) the hydrogen reversible potential and (ii) the water/Pt(100) ionization potential (IP) relative to the thermodynamic work function [36] of the standard hydrogen electrode. By definition, gaseous $1/2H_2$ is in equilibrium with $(H_3O^+ + e^-)$ at water/Pt(100) interface at the reversible potential. Therefore, in our method, the charge q where the energy of gaseous $1/2H_2$, solvated H_3O^+, and e^- in the metal electrode are equal corresponds to the hydrogen reversible potential. At this potential, E_a of the Volmer step in the hydrogen oxidation ($H_{ads} \rightarrow H_3O^+ + e^-$) and hydrogen evolution ($H_3O^+ + e^- \rightarrow H_{ads}$) reactions is also equal. Similar to our calculations with cluster models of the water/Pt(111) [21] and water/Pt(110) [29] interfaces, the reversible potential for the water/Pt(100) interfaces is near q=−2 (Figs. 6 and 9) and the IP relative to RHE is ca. +0.2 V for the water/Pt(100) interface.

Minimum energy pathways were determined approximately with an elastic band method. The points in the band were generated gradually connecting reactants and products. Each point is partially optimized minimizing forces and energy. The approximate transition state structures were checked by a normal mode analysis to exhibit a single imaginary frequency.

The direct MD method employed in the present work has been developed and implemented in our group [21]. The method is a quantum-classical simulation where at each time step the energy gradient in the classical evolution of the atomic nuclei is evaluated with an electronic structure approach, e.g., DFT. The hydrogen oxidation is a proton-coupled electron-transfer reaction and non-adiabatic quantum effects are non-negligible [37]. We, however, treated all nuclei classically. Instead of fitting the potential surface to an analytic form beforehand, we generated it "on the fly." In this way, we avoid the complications of constructing an accurate surface. Generating the surface on the fly restricts the dynamics of reactive systems from being examined in as much detail as they can be on a fitted surface. However, the direct MD is a more practical approach for large complex systems.

The classical equation of motion in our MD was integrated using the Verlet algorithm with a time step of 0.5 femtoseconds (fs). DMol [3] was employed to evaluate the energies and gradients with DFT calculations. All water molecules and the H_2 molecule began each direct MD trajectory with vibrational but no rotational energy. Zero-point vibrational energy was not given to the Pt cluster. During the direct MD simulation, the water molecules, hydrogen atoms and the top layer of the Pt clusters were allowed to move freely. The bottom layer of the Pt clusters was held fixed to the experimental position of bulk Pt. A number of trajectories with initial H_2-Pt(100) separations ranging from 2.5 to 3.5 Å were chosen and each one lead to dissociative H_2. The 18 water molecules allowed the H^+ oxidation product to fluctuate between a variety of structures, such as $H_5O_2^+$ (Zundel ion) and $H_9O_4^+$ [38].

Results and Discussion

The main features of the voltammogram of well-ordered Pt(100) in acid solution, e.g., 0.05 M H_2SO_4 [6], are two delineated peaks at ca. +0.25 and +0.4 V vs. RHE. The +0.25 and +0.4 V peaks have been associated with the coupling of hydrogen adsorption/desorption with the anion desorption/adsorption on the $n(100)\times(111)$ step sites and (100) terrace sites, respectively [6]. In the present work, we are mainly interested in the HOR at potentials below +0.2 V vs. RHE. Therefore, the effects of anion adsorption have not been considered. We focused our study on the (100) terrace sites,

although the $n(100)\times(111)$ step site was also studied to a lesser extent.

The HOR on Pt electrodes is very sensitive to the electrode potential [16, 21, 28, 29]. Moreover, at low overpotential, the Pt surface is covered with spectator-adsorbed hydrogen, and the HOR is expected to take place under high coverage of adsorbed hydrogen [39, 40]. We studied the effect of hydrogen coverage and electrode potential on the HOR on Pt(100), performing two series of calculations: (i) HOR at low coverage of adsorbed hydrogen at ca. 0.0 and +0.2 V vs. RHE and (ii) HOR at ca. 1 ML coverage of adsorbed hydrogen at ca. 0.0 V vs. RHE.

The high coverage of hydrogen under electrochemical conditions have been recently studied on Pt(111) [26, 28, 34], Pt(110) [26, 29, 34], and Pt(100) [26, 34]. The state of adsorbed hydrogen at high coverage, i.e., the UPD state of hydrogen, on Pt(111) and Pt(110), is still controversial as it has been identified by different calculations as hydrogen on bridge [21, 28], and hollow site [20, 24, 26] on Pt(111) and hydrogen on-top [29] and bridge [26] sites on the outmost Pt row in Pt(110). The situation is different for Pt(100). A previous study by Skulason et al. [26] found hydrogen to be stable on the bridge site, reaching up to 2 ML, two hydrogen atoms per Pt site, on Pt(100). We also found hydrogen on bridge sites over Pt(100) as the most stable configuration with a maximum coverage of 2 ML. We, therefore, do not discuss further our results for the UPD state of hydrogen on Pt(100) as they are similar to previous calculations [26].

We start our discussion with the results for the direct MD and MEP of HOR at the Pt(100) terrace site. We then turn to discuss E_a of the HOR on terrace and step sites as a function of electrode potential and end the discussion with the predicted Tafel plot for hydrogen reactions on Pt(100) terrace sites.

Direct Molecular Dynamics of the HOR

We first explored the mechanism of the HOR performing molecular dynamics simulations of the reaction of H_2 at the terrace sites of the Pt(100)/water interface. The reaction was studied under three electrochemical conditions: (i) low coverage of adsorbed hydrogen at ca. 0.0 V vs. RHE, (ii) ca. 1 ML coverage of adsorbed hydrogen at ca. 0.0 V vs. RHE, and (iii) low coverage of adsorbed hydrogen at ca. +0.2 V vs. RHE. A sequence of configurations in the H_2-Pt(100) surface reaction under the electrochemical conditions i, ii, and iii are shown in Figs. 2, 3, and 4, respectively. These trajectories represent reactive surface processes in which the solvated H_2 molecule makes side-on and end-on approaches to the Pt(100) surface at low and high hydrogen coverage.

The reaction mechanism is straightforward, similar to other water/Pt interfaces [21, 29]. Initially, the H_2 molecule is drawn to the metal surface by the attractive interaction with Pt. Subsequently, a rapid bond-breaking process takes place. This process is common around 5 fs to all electrochemical conditions and trajectories (Figs. 2, 3, and 4). Above 5 fs, the dynamics depend on the electrochemical conditions. The dissociation takes place easily because H_2 does not need to displace surface water molecules [41]. Near the reversible potential, water molecules are not bound to Pt, as we and other have previously reported (see Ref. [42] and references therein).

At low overpotential and low surface hydrogen coverage (Fig. 2), a highly exothermic non-oxidative adsorption forms two H_b on the surface. The exothermic energy is imparted to the kinetic energy of one of the H_b that undergoes a rapid site-to-site shift and to the excitations in the wagging vibrational mode of the other H_b (30–55 fs). The Tafel process dominates the HOR on Pt(100) at low overpotential and low hydrogen surface coverage. Under these electrochemical conditions, the majority of trajectories that were examined showed a non-oxidative adsorption of H_2 similar to that displayed in (Fig. 2). The oxidation of H_b at the water/Pt(100) interface will seldom take place because it requires a high E_a of 6.9 kcal/mol, see discussion in the next section. The Tafel process at low overpotential and low surface hydrogen coverage results in the deposition of hydrogen (i.e., UPD hydrogen) on the Pt(100) surface.

The HOR via the Heyrovsky-Volmer process begins to take place only when the Pt(100) surface reaches ca. 1 ML H_b coverage or when the electrode overpotential is increased. At ca. 1 ML H_b coverage, where the adsorbed hydrogen tends to block the Tafel process or further deposition of two additional H_b (Fig. 3), the heterolytic dissociation of H_2 takes place to form a proton and H_b on the femtosecond time scale (10–20 fs). This was followed by a site-to-site shift of H_b.

H_2 follows a similar dissociative oxidation pathway at the intermediate overpotential of ca. +0.2 V vs. RHE even at low hydrogen surface coverage (Fig. 4). Thus, the direct dissociative oxidation of H_2 via the Heyrovsky-Volmer process is found to be the minimum energy pathway for the HOR at ca. 1 ML H_b coverage at low overpotential as well as at low hydrogen coverage and higher electrode potentials; results are shown in Fig. 5. In both of these electrochemical conditions, H_2 spontaneously dissociates to form a proton and H_b.

Our results can help to rationalize the current density experimentally observed near the reversal potential in the Pt(100) voltammogram [40]. Under experimental conditions at low overpotential, the Pt(100) and Pt(111) surfaces are known [26, 34] to be covered with adsorbed hydrogen. According to our molecular dynamics simulations and minimum energy pathway calculations, the HOR on the Pt(100) surface takes place at Pt sites that are partially covered with nonreactive adsorbed hydrogen. This contrasts with the HOR on the Pt(111) surface, where the inactive adsorbed hydrogen saturate [26, 28] the surface at low overpotential and blocks the active Pt sites. As a result, no current density is observed near the reversible potential in the Pt(111) voltammogram [40].

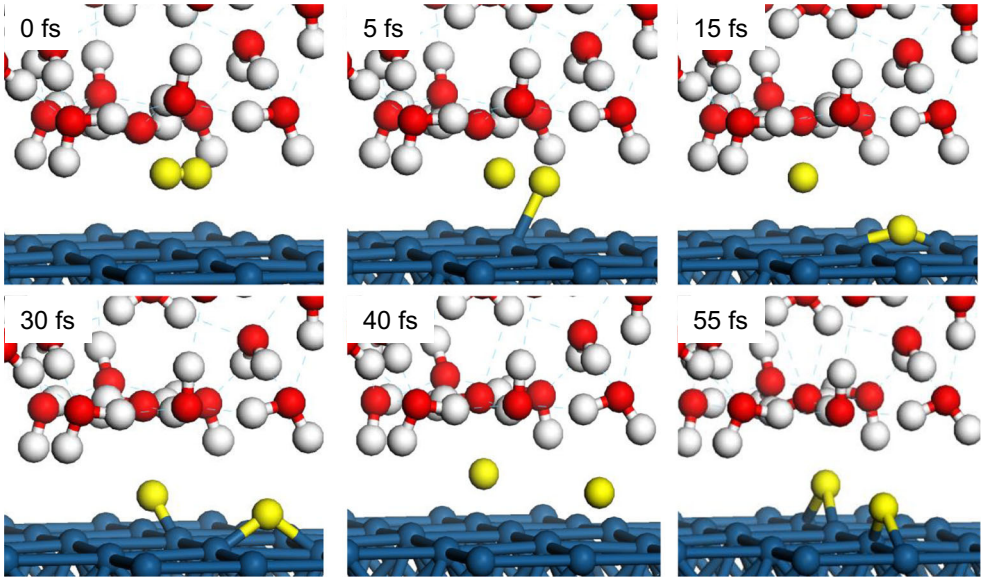

Fig. 2 A sequence of atomic configurations in a sample MD trajectory of the Tafel step in H_2 oxidation on Pt(100) terraces sites at low coverage (in the absence) of adsorbed hydrogen at ca. 0.0 V vs. RHE. $H_2/2H_b$ is highlighted in yellow

Reversible Electrode Potential

To better understand the results of our molecular dynamics for the HOR near the reversible potential, we evaluated the H_2/Pt(100)/water potential energy surface to establish the minimum energy pathway. A relative energy diagram is shown in Fig. 6 for H_2/Pt(100)/water at low coverage of adsorbed hydrogen at ca. 0.0 V vs. RHE. As expected, the energy of $1/2H_{2(g)}$ is close to that of $(H_3O^+ + e^-)$ near the reversible potential. In line with the molecular dynamics results at ca. 0.0 V vs. RHE, the minimum energy pathway calculations show that the H_2 dissociation is barrierless and exothermic by 15 kcal/mol. The homolytic H-H bond breaking forms two H_b with an average interatomic Pt-H distance of 1.72 Å. The vibrational frequency for the stretching mode of H_b is calculated at 1467 cm^{-1}, after correcting for anharmonicity [43]. The energy released upon the dissociation goes into the product internal energy, resulting in the site-to-site shift and vibrational excitation of H_b observed in the molecular dynamics (Fig. 2). The rapid site-to-site diffusion of H has been also established for other Pt surfaces [44].

H_b interacts very little with solution water; the interatomic H_b-$(H_2O)_{sol}$ distances are over 3 Å. The HOR of H_b, therefore, can take place only when H_b is activated and isomerized to an on-top hydrogen H_o. We found an E_a of 6.9 kcal/mol for this isomerization (Fig. 6) on the water/Pt(100) interface at low hydrogen coverage. This relatively high E_a comes in part from the different binding energy of H_b (68 kcal/mol) and H_o (63 kcal/mol) and helps to explain the absence of an oxidative pathway at low coverage of adsorbed hydrogen at ca. 0.0 V vs.

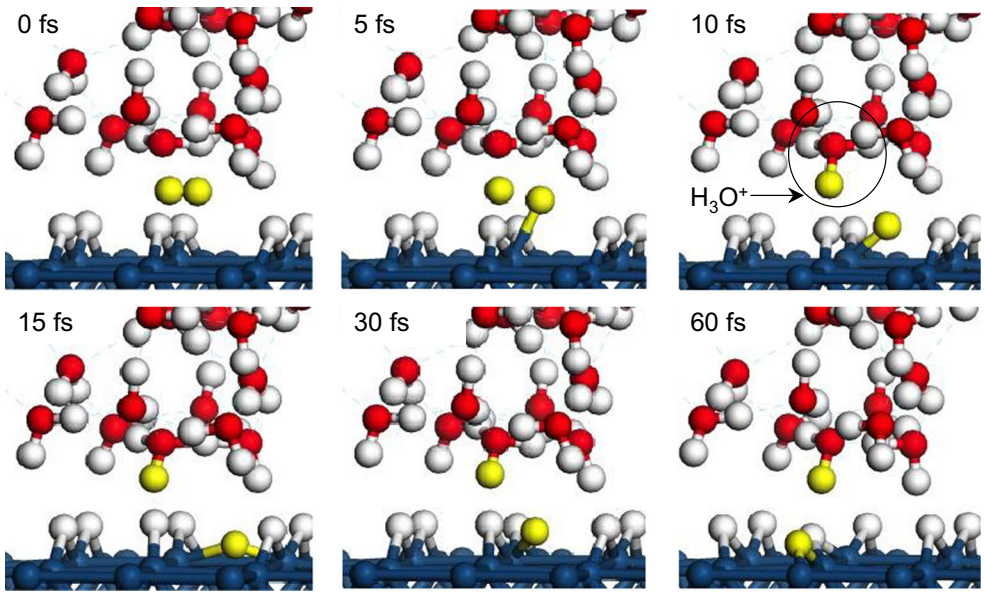

Fig. 3 A sequence of atomic configurations in a sample MD trajectory of the Heyrovsky-Volmer process in H_2 oxidation on Pt(100) terrace sites at ca. 1 ML coverage of adsorbed hydrogen at ca. 0.0 V vs. RHE. $H_2/2H$ is highlighted in *yellow*

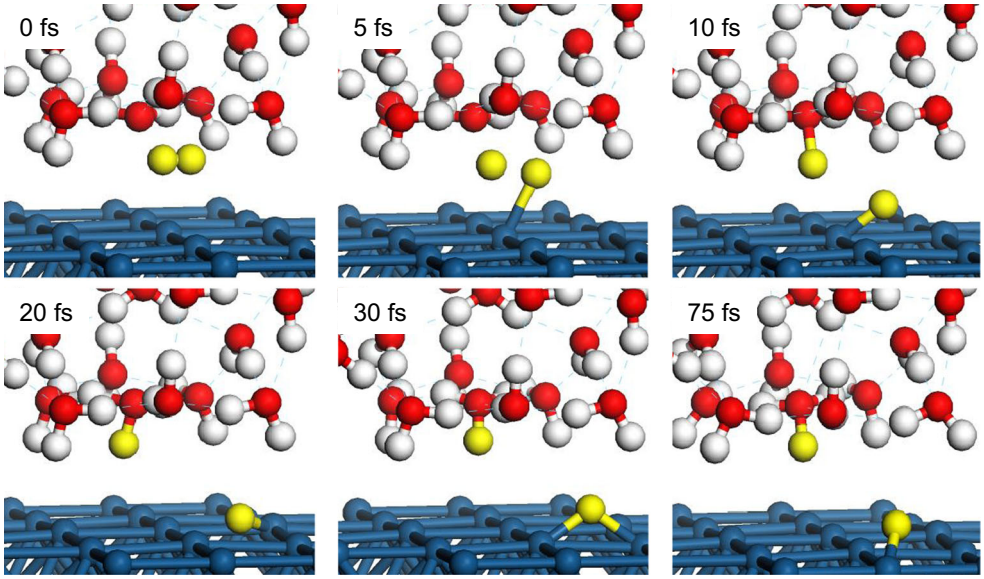

Fig. 4 A sequence of atomic configurations in a sample MD trajectory of the Heyrovsky-Volmer process in H_2 oxidation on Pt(100) terrace sites at low coverage of adsorbed hydrogen at ca. +0.2 V vs. RHE. H_2/2H is highlighted in *yellow*

RHE within the time frame of our direct molecular dynamics simulations. Once H is in an on-top position (H_o; Fig. 6), a hydrogen bond with an interatomic H_o-$(OH_2)_{sol}$ distance of ca. 1.73 Å is formed. The vibrational frequency for the stretching mode of H_o is 2023 cm^{-1}. The direct interaction of H_o with solution water allows the oxidation of H_o via the Volmer process. The oxidation, however, is not spontaneous; E_a is 1.7 kcal/mol (Fig. 6).

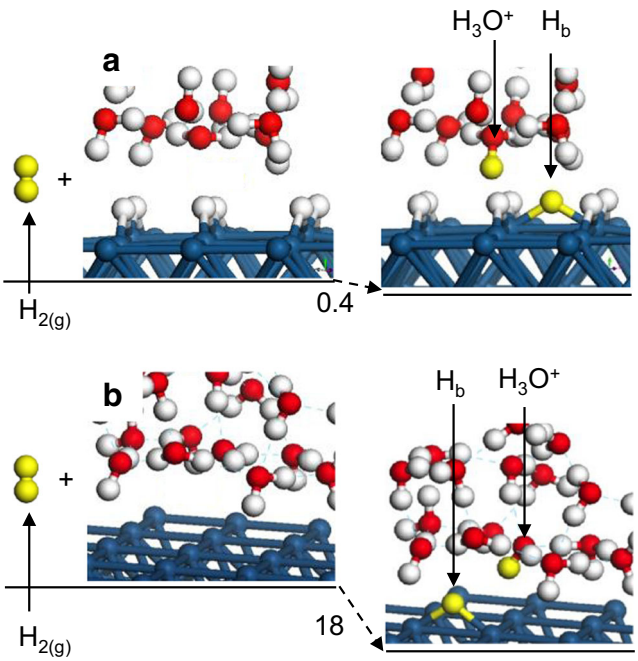

Fig. 5 Relative energy diagram of the Heyrovsky-Volmer pathway of the H_2 oxidation at **a** ca. 1 ML coverage of adsorbed hydrogen at ca. 0.0 V vs. RHE and **b** low coverage of adsorbed hydrogen at ca. +0.2 V vs. RHE on Pt(100) terrace sites. H_2/2H is highlighted in yellow. The reaction energy is given in kcal/mol

As shown in Figs. 7a and 8, E_a for the $H_o \rightarrow H_3O^+ + e^-$ Volmer oxidation step and the $H_b \rightarrow H_o$ isomerization step on Pt(100) terrace sites, respectively, depend on the electrode potential. The potential where E_a for the forward ($H_o \rightarrow H_3O^+ + e^-$) and reverse ($H_3O^+ + e^- \rightarrow H_o$) reactions are equal (the crossing point in Fig. 7a) is achieved at $q \sim -2$. This E_a and the crossing potential are rather insensitive to the surface hydrogen coverage. At the crossing potential, E_a is close to 1.7 kcal/mol at low and ca. 1 ML hydrogen coverage. The value of 1.7 kcal/mol was determined by interpolation. As mentioned in Computational Details, this crossing potential corresponds to the reversible potential (i.e., 0.0 V vs. RHE) when gaseous $1/2H_2$ is in equilibrium with ($H_3O^+ + e^-$). As shown in (Fig. 5a), gaseous $1/2H_2$ is in equilibrium with ($H_3O^+ + e^-$) when the hydrogen coverage is ca. 1 ML. At low coverage, however, the gaseous $1/2H_2$ state is not in equilibrium with the ($H_3O^+ + e^-$) state (Fig. 6).

E_a for the isomerization at terrace sites on Pt(100) near 0.0 V vs. RHE are 6.9 and 5.6 kcal/mol at low and ca. 1 ML hydrogen coverage, respectively. As the overpotential is increased, i.e., added positive charge, E_a for the oxidation step decreases, vanishing at $q = -1$ (ca. +0.1 V vs. RHE) for hydrogen coverage of ca. 1 ML. Similarly, E_a for the $H_b \rightarrow H_o$ isomerization decreases with increasing overpotential, but it does not vanish and instead reaches a value of ca. 2.7 kcal/mol at potentials of ca. +0.4 V vs. RHE and hydrogen coverage of ca. 1 ML (Fig. 8).

The HOR does not only take place at terrace sites but also at steps sites on the Pt(100) surface [6]. We, therefore, evaluated the minimum energy pathway of HOR at the (111) step site of Pt(100) as well. A relative energy diagram is shown in Fig. 9 for H_2/water/stepped Pt(100) at low coverage of adsorbed hydrogen at ca. 0.0 V vs. RHE. Hydrogen dissociation at the step sites follows an exothermic non-oxidative

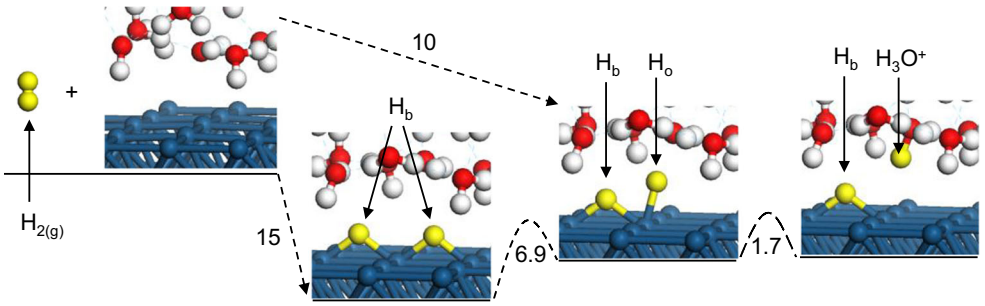

Fig. 6 Relative energy diagram of the Tafel-Volmer pathway of the H_2 oxidation at low coverage of adsorbed hydrogen at ca. 0.0 V vs. RHE on Pt(100) terrace sites. H_2/2H is highlighted in *yellow*. Reaction and activation energies are given in kcal/mol

adsorption forming two H_b on the outmost step Pt atoms. H_b on the step site has an asymmetry structure with interatomic Pt-H_b distances of 1.66 and 1.78 Å. The vibrational frequency for the stretching mode of H_b ranges from 1601 to 1829 cm^{-1}. Similar to the H_b on terrace sites, the interatomic H_b-$(H_2O)_{sol}$ distances are over 3 Å for H_b on the step site. H_b on the step site, therefore, does not interact strongly with solution water.

The oxidation of H_2 on step sites at low coverage of adsorbed hydrogen at 0.0 V vs. RHE also requires the activation and isomerization of adsorbed hydrogen from the bridge to the on-top site. E_a for the H_b to H_o isomerization is insensitive to the electro potential (Fig. 8) in the case of step sites, with a value of ca. 4.5 kcal/mol. H_o on the step site has a Pt-H_o distance of 1.55 Å and a vibrational frequency for the stretching mode of 1991 cm^{-1}. H_o on the step site also forms a hydrogen bond with solution water; with a distance of 1.83 Å. Similar to the HOR on terrace sites, the $H_o \rightarrow H_3O^+ + e^-$ Volmer mechanism on step sites depends on the electrode potential (Fig. 7b). E_a at the reversible potential is coincidentally also 1.7 kcal/mol.

The calculated E_a for the oxidation of UPD hydrogen, $H_b \rightarrow H_o \rightarrow H_3O^+ + e^-$, at the reversible potential on Pt(100) at terrace and step sites, 6.9 and 4.5 kcal/mol, respectively, are much higher than the measured [6] value of 2.87 kcal/mol. This is in contrast with the oxidation of UPD hydrogen

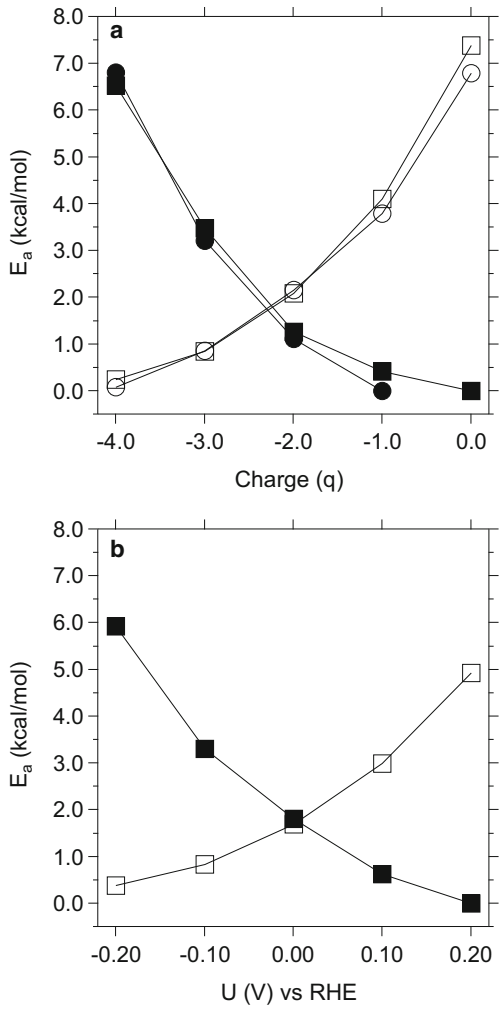

Fig. 7 Activation energy (E_a) for the Volmer step in the hydrogen oxidation ($H_o \rightarrow H_3O^+ + e^-$, *closed symbols*) and hydrogen evolution ($H_3O^+ + e^- \rightarrow H_o$, *open symbols*) reactions as a function of the electrode potential (or added Charge q) at the water/Pt(100) interface. Results are shown for **a** Pt(100) terrace sites at low (*square symbols*) and ca. 1 ML (*circle symbols*) coverage of adsorbed hydrogen and for **b** Pt(100) with (111) step sites at low coverage of adsorbed hydrogen

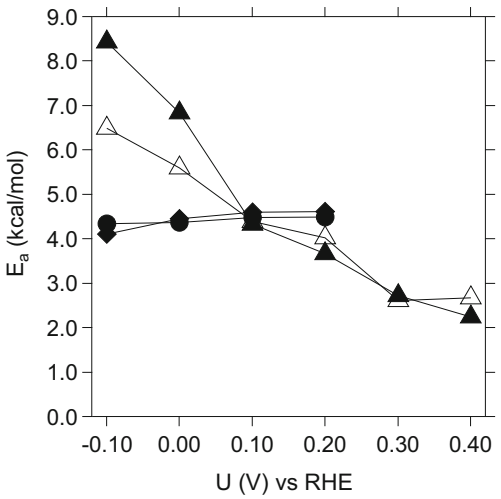

Fig. 8 Activation energy (E_a) for the isomerization of bridging hydrogen, H_b, to on-top hydrogen, H_o, ($H_b \rightarrow H_o$) as functions of the electrode potential at the Pt(100) terrace (*triangle symbols*) and (111) step (*circle symbols*) sites. Results for the isomerization of H_b at Pt(111) terrace sites are also included (*diamond symbols*) for comparison. For the isomerization at the Pt(100) terrace sites, results are shown for low (*closed triangle symbols*) and ca. 1 ML (*open triangle symbols*) coverage of adsorbed hydrogen

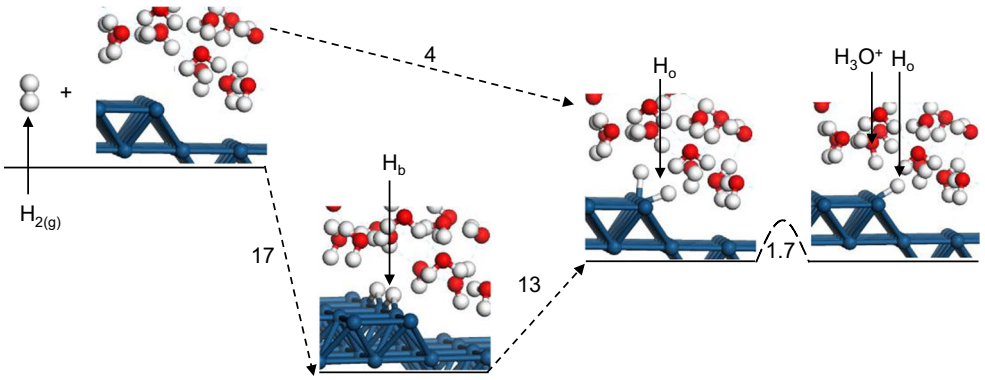

Fig. 9 Relative energy diagram of the Heyrovsky-Volmer pathway of the H_2 oxidation at low coverage of adsorbed hydrogen at ca. 0.0 V vs. RHE on Pt(100) with (111) step sites. Reaction and activation energies are given in kcal/mol

on Pt(111) and Pt(110). To compare with Pt(100), we also studied the $H_b \rightarrow H_o$ isomerization on Pt(111); results are included in (Fig. 8). The calculated E_a for the oxidation of UPD hydrogen on Pt(111) is ca. 4.5 kcal/mol, which is rather insensitive to the electrode potential. This value agrees with the measured [6] value of 4.3 kcal/mol. E_a for the oxidation of UPD hydrogen on Pt(110) is 2.3 kcal/mol [29], in agreement with the measured [6] value of 2.27 kcal/mol. It is likely that E_a, 2.87 kcal/mol [6], determined experimentally is not for the oxidation of UPD hydrogen, H_b, but for the oxidation of H_o generated in the Heyrovsky-Volmer process.

Our results show that the oxidation of UPD hydrogen on Pt(111) and Pt(100) differ from that on Pt(110). On Pt(110), where hydrogen is stable only at on-top position [29], the oxidation of UPD hydrogen taking place via the $H_o \rightarrow H_3O^+ + e^-$ Volmer mechanism with a low E_a. The low E_a result in a high HOR activity in this surface, as indicated by the high current density in the Pt(110) voltammogram [29]. On the other hand, UPD hydrogen is at bridge position on Pt(111) and Pt(100). The oxidation of UPD hydrogen on these surfaces proceeds via the $H_b \rightarrow H_o \rightarrow H_3O^+ + e^-$ mechanism. As shown above, the $H_b \rightarrow H_o$ isomerization step requires relatively high E_a, resulting in the low current density observed in the UPD region in the voltammogram of these surfaces [29]. The current density is particularly low for Pt(100) where E_a for the $H_b \rightarrow H_o$ isomerization is relatively high.

Tafel Plot

As in our previous work [29], here we employed the calculated electrode potential-dependent E_a for H_2 oxidation on Pt(100) to predict the Tafel plot in the spirit of Anderson and Cai [16]. In the low overpotential region, where oxidation and reduction reactions would contribute nearly equally [16], the total current density i may be given by $i = i_{ox} + i_{red} = A(\exp[E_a^{ox}(U)/RT] + \exp[E_a^{red}(U)/RT])$, where i_{ox} and i_{red} are, respectively, oxidation and reduction kinetic current density. The pre-exponential factor A is proportional to a number of variables, such as the concentration of adsorbed hydrogen/proton undergoing oxidation/reduction, the frequency factor, and the Faraday constant. T is the temperature of the system. $E_a(U)$ is the activation energy at a potential U for oxidation or reduction.

E_a for the Volmer step in the $H_o \rightarrow H_3O^+ + e^-$ oxidation and $H_3O^+ + e^- \rightarrow H_o$ reduction reactions at ca. 1 ML coverage of surface hydrogen on Pt(100) (Fig. 7a) were fitted to third order polynomial equations and employed to predict the Tafel plot. The predicted Tafel plot is shown in Fig. 10 along with the experimental Tafel plot at 274 K [6]. The experimental plot is reproduced with the pre-exponential factor $A = 16$. We fitted the curve with slopes of 51 and 110 mV/decade. Extrapolation of the 51 mV/decade slope results in an exchange current density $i_0 = 0.37$ mA cm^{-2}, in agreement with the measured [6] value of 0.36 mA cm^{-2}. The calculated slope of 110 mV/decade also agrees with the measured value of 112 mV/decade (Fig. 4 in Ref. [6]). The other calculated slope (51 mV/decade), however, deviates from the value of 37 mV/decade reported in Ref. [6]. Graphically analyzing the Tafel slopes shown in Fig. 4 of Ref. [6] for Pt(100), we found that the numerical value reported, 37 mV/decade, is not the slope of

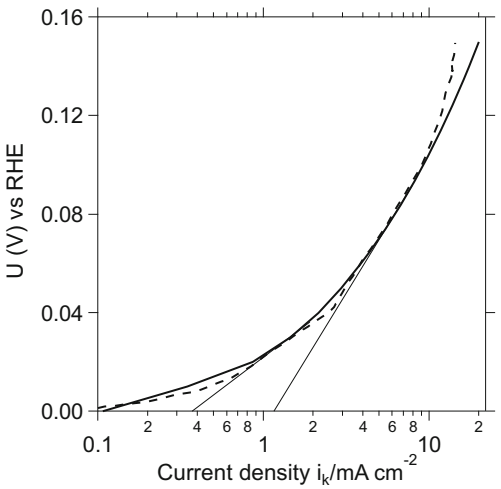

Fig. 10 Tafel plot for hydrogen oxidation at Pt(100) terrace site at 274 K. The *dashed curve* corresponds to experimental results of Ref. [6] and the *full curve* to our prediction employing the activation energy of the hydrogen oxidation/reduction at ca. 1 ML coverage of adsorbed hydrogen (Fig. 7a). The *curve* was fitted with two Tafel slopes

the line shown in the figure. The slope in the figure is instead 46 mV/decade, in closer agreement with our calculated value. No differences were found for the slope of 112 mV/decade. The agreement of the calculated and measured Tafel slopes and exchange current density i_0 for hydrogen reactions on Pt(100) strongly supports that the electro-oxidation takes place via the Heyrovsky-Volmer mechanism [16].

Conclusions

In the present work, we have employed the first-principles-based molecular dynamics to bring atomic-level insight into the hydrogen electro-oxidation at the Pt(100)/water interface. We studied the effect of inactive adsorbed hydrogen and electrode potential on the electro-oxidation reaction studying the oxidation at low coverage of adsorbed hydrogen at (i) ca. 0.0 V vs. RHE and (ii) ca. +0.2 V vs. RHE, and (iii) at ca. 1 ML coverage of adsorbed hydrogen at ca. 0.0 V vs. RHE. At ca. 0.0 V vs. RHE, the electro-oxidation follows the Tafel-Volmer homolytic cleavage of H_2 if the coverage of adsorbed hydrogen is low, and the Heyrovsky-Volmer mechanism if the surface is covered with ca. 1 ML of hydrogen. At potential of ca. +0.2 V vs. RHE, the oxidation proceeds via the Heyrovsky-Volmer mechanism independently of the surface hydrogen coverage. Good agreement between measured and predicted Tafel plots also indicates that hydrogen oxidation/reduction reaction on Pt(100) proceeds via the Heyrovsky-Volmer mechanism under ca. 1 ML coverage of inactive adsorbed hydrogen.

We have also studied the oxidation of UPD H on Pt(100). In agreement with previous calculations by Skulason et al. [26], we identified UPD H as hydrogen in the bridging position on Pt(100). The electro-oxidation of UPD H at terrace sites on Pt(100) requires the isomerization of hydrogen from bridge to on-top position. This surface transformation has a high activation energy, and it is likely to be the rate-determining step in the electro-oxidation of UPD H on the Pt(100) and Pt(111) surfaces.

Acknowledgments This work was supported by the NASA-UPR Center for Advanced Nanoscale Materials.

Author Contributions The manuscript was written through contributions of all authors. All authors have given approval to the final version of the manuscript.

References

1. G. Jerkiewicz, Electrocatalysis **1**(4), 179–199 (2010)
2. A. Wieckowski, J.K. Nørskov, A. Wieckowski (eds.), *Fuel Cell Science: theory, fundamentals, and biocatalysis*, Seriesth edn. (John Wiley & Sons, Inc, New Jersey, 2010)
3. R.J. Nichols, A. Bewick, J. Electroanal. Chem. Interfacial. Electrochem. **243**(2), 445–453 (1988)
4. R. Gomez, A. Fernandez-Vega, J.M. Feliu, A.J. Aldaz, Phys. Chem. **97**(18), 4769–4776 (1993)
5. N.M. Markovića, S.T. Sarraf, H.A. Gasteiger, P.N. Ross, J. Chem. Soc. Faraday Trans. **92**(20), 3719–3725 (1996)
6. N.M. Marković, B.N. Grgur, P.N. Ross, J. Phys. Chem. B **101**(27), 5405–5413 (1997)
7. A. Peremans, A.J. Tadjeddine, Chem. Phys. **103**(16), 7197–7203 (1995)
8. B. Ren, X. Xu, X.Q. Li, W.B. Cai, Z.Q. Tian, Surf. Sci. **427**, 157–161 (1999)
9. N. Nanbu, T.J. Ohsaka, Electroanal. Chem. **485**(2), 128–134 (2000)
10. K. Kunimatsu, T. Senzaki, G. Samjeské, M. Tsushima, M. Osawa, Electrochim. Acta **52**(18), 5715–5724 (2007)
11. H. Ogasawara, M. Ito, Chem. Phys. Lett. **221**(3–4), 213–218 (1994)
12. M. Nakamura, T. Kobayashi, N. Hoshi, Surf. Sci. **605**(15–16), 1462–1465 (2011)
13. E. Santos, W. Schmickler, in *Catalysis in Electrochemistry*, ed. by E. Santos, W. Schmickler (John Wiley & Sons, Inc, Hoboken, 2011), pp. 197–222
14. A. Gross, S. Schnur, in *Catalysis in Electrochemistry*, ed. by E. Santos, W. Schmickler (John Wiley & Sons, Inc, Hoboken, 2011), pp. 165–196
15. P. Ferrin, M. Mavrikakis, J. Rossmeisl, J.K. Nørskov, in *Fuel cell science*, ed. by A. Wieckowski, J.K. Nørskov (John Wiley & Sons, Inc, Hoboken, 2010), pp. 489–510
16. A.B. Anderson, Y. Cai, J. Phys. Chem. B **108**(52), 19917–19920 (2004)
17. J. Greeley, J.K. Nørskov, L.A. Kibler, A.M. El-Aziz, D.M. Kolb, ChemPhysChem **7**(5), 1032–1035 (2006)
18. C. Taylor, S. Wasileski, J.-S. Filhol, M. Neurock, Phys. Rev. B **73**(16), 165402 (2006)
19. O. Sugino, I. Hamada, M. Otani, Y. Morikawa, T. Ikeshoji, Y. Okamoto, Surf. Sci. **601**(22), 5237–5240 (2007)
20. E. Skúlason, G.S. Karlberg, J. Rossmeisl, T. Bligaard, J. Greeley, H. Jónsson, J.K. Nørskov, Phys. Chem. Chem. Phys. **9**(25), 3241 (2007)
21. Y. Ishikawa, J.J. Mateo, D.A. Tryk, C.R.J. Cabrera, Electroanal. Chem. **607**(1–2), 37–46 (2007)
22. J. Rossmeisl, E. Skúlason, M.E. Björketun, V. Tripkovic, J.K. Nørskov, Chem. Phys. Lett. **466**(1–3), 68–71 (2008)
23. E. Santos, A. Lundin, K. Pötting, P. Quaino, W.J. Schmickler, Solid State Electrochem. **13**(7), 1101–1109 (2008)
24. I. Hamada, Y. Morikawa, J. Phys. Chem. C **112**(29), 10889–10898 (2008)
25. R. Jinnouchi, A.B. Anderson, J. Phys. Chem. C **112**(24), 8747–8750 (2008)
26. E. Skúlason, V. Tripkovic, M.E. Björketun, S. Gudmundsdóttir, G. Karlberg, J. Rossmeisl, T. Bligaard, H. Jónsson, J.K. Nørskov, J. Phys. Chem. C **114**(42), 18182–18197 (2010)
27. J. Rossmeisl, K. Chan, R. Ahmed, V. Tripković, M.E. Björketun, Phys. Chem. Chem. Phys. **15**(25), 10321 (2013)
28. J.J. Mateo, D.A. Tryk, C.R. Cabrera, Y. Ishikawa, Mol. Simul. **34**(10–15), 1065–1072 (2008)
29. J.A. Santana, J.J. Mateo, Y. Ishikawa, J. Phys. Chem. C **114**(11), 4995–5002 (2010)
30. B. Delley, J. Chem. Phys. **113**(18), 7756–7764 (2000)
31. J.P. Perdew, K. Burke, M. Ernzerhof, Phys. Rev. Lett. **77**(18), 3865–3868 (1996)
32. K. Christmann, in *Electrocatalysis*, ed. by J. Lipkowski, P.N. Ross (Wiley-VCH, New York, 1998), p. 1
33. R. Gómez, J.M. Orts, B. Álvarez-Ruiz, J.M. Feliu, J. Phys. Chem. B **108**(1), 228–238 (2004)
34. N. Garcia-Araez, J. Phys. Chem. C **115**(2), 501–510 (2011)

35. A. Zolfaghari, M. Chayer, G.J. Jerkiewicz, Electrochem. Soc. **144**(9), 3034–3041 (1997)
36. S. Trasatti, Pure Appl. Chem. **58**(7), 955–966 (1986)
37. C. Venkataraman, A.V. Soudackov, S. Hammes-Schiffer, J. Phys. Chem. C **112**(32), 12386–12397 (2008)
38. D. Marx, M.E. Tuckerman, J. Hutter, M. Parrinello, Nature **397**(6720), 601–604 (1999)
39. D.S. Strmcnik, P. Rebec, M. Gaberscek, D. Tripkovic, V. Stamenkovic, C. Lucas, N.M. Marković, J. Phys. Chem. C **111**(50), 18672–18678 (2007)
40. D. Strmcnik, D. Tripkovic, D. van der Vliet, V. Stamenkovic, N.M. Marković, Electrochem. Commun. **10**(10), 1602–1605 (2008)
41. G. Jerkiewicz, G. Vatankhah, S. Tanaka, J. Lessard, Langmuir **27**(7), 4220–4226 (2011)
42. J.A. Santana, Y. Ishikawa, Electrochim. Acta **56**(2), 945–952 (2010)
43. J.P. Merrick, D. Moran, L. Radom, J. Phys. Chem. A **111**(45), 11683–11700 (2007)
44. G.W. Watson, R.P.K. Wells, D.J. Willock, G.J. Hutchings, J. Phys. Chem. B **105**(21), 4889–4894 (2001)